Self-Assembly of Octahedral Patchy Particles

Serwan Asaad
Supervisor: Laura Filion

January 18, 2013

Abstract

In this thesis the equilibrium behaviour of colloidal particles decorated with patches in an octahedral arrangement have been studied through the use of Monte Carlo (MC) simulations. The patches of the particles have a patch-antipatch interaction type, i.e. each patch can only form bonds with a specific antipatch on other particles. For these particles the fluid, simple cubic (sc) crystal and body-centered-cubic (bcc) crystal phases have been studied. Through MC simulations in the constant number of particles, pressure and temperature ensemble the equation of state has been found and via Einstein integration the free energies of the phases have been found. Combining these two results the phase diagram of the particles has been determined for number densities between $\rho\sigma^3 = 0$ and $\rho\sigma^3 = 1.2$, where σ is the particle's diameter. It has been found that three phases are stable for temperatures between $k_bT = 0.2$ and $k_bT = 0.35$, where k_b is Boltzmann's constant. It is expected that at higher temperatures the face-centered-cubic crystal (fcc) phase is expected to be stable, although this has not been explored in this paper. At higher temperatures (above $k_bT = 0.35$) melting of both crystal phases has been observed.

Contents

1 Introduction

The concept of particles decorated with attractive patches, also known as patchy particles, was first examined theoretically around 1980 as a way of studying the behaviour of molecules such as water and silica. In these models the attractive patches mimick the interaction between the atoms in the molecules. For instance, the behaviour of fluids has been studied by Smith et al. [12] by using a crude model in which the patches represent hydrogen bonds.

In more recent years interest has been renewed in the patchy particle model. One of the main reasons for this renewed interest in patchy particles is due to the fact that experimental scientists have been able to produce colloids with attractive patches. Colloids are particles whose sizes are between a nanometer to a few microns and exhibit Brownian motion. There are now several techniques to create patches on colloids. One of these techniques is called Glancing Angle Deposition (GLAD). Here particles arranged in a periodic structure are coated by a vapor at an angle, causing each particle to partly shield its neighbour from the coating. This results in particles being partly covered by the coating, effectively creating a patch on each particle. By varying the angle, coating, etc. the shape and properties of the patches can be modified. This technique has been applied by Pawar and Kretzschmar[8] who have been able to succesfully create particles covered by two patches which further overlap each other by 1.6%.

A second technique for the synthesis of patchy colloids is called Templating. In this technique colloids are placed at the interface between two phases. One of the phases is called the template and is meant to cover the section of the colloids that are in it. The other phase is then introduced to reagents which then modify the surface of the colloids. Since the reagents have only been able to modify the non-templated surface of the particles, the colloids are finally left with a patch.

One very interesting property of patchy particles is the influence the patches have on the crystallization of the particles. The ability to introduce patches to colloidal particles in a specific arrangement can promote self-assembly into certain crystal structures. This opens up new possibilities in designing colloidal crystals. One important application of colloidal crystals is their use as a photonic crystal. Photonic crystals behave the same way for photons as semiconductors behave for electrons. It comes as no surprise that being able to design colloidal crystals is therefore of great importance

for the field of photonics.

Another reason for the renewed interest in patchy particle systems is due to the fact that it is a basic model for studying the behaviour of proteins crystallization. Determining the structure of a protein is most often done through x-ray crystallography. To be able to apply this technique a necessary condition is that the protein must be crystallized. However there are many issues surrounding the crystallization of proteins, such as the solution parameters. As noted by Chang et al.[1], "The biophysics of protein interactions, and the similarity in the phase behavior of protein and colloid solutions, suggest that the protein interactions are short-ranged compared to the size of the protein." For this reason the bonding between proteins can be approximated by introducing patches to particles.

Alongside experimental findings computer simulations have also given new insights into the behaviour of patchy particles. An advantage of simulations is that the parameters of the particles and their patches can be modified relatively easy and with great precision compared to physical experiments. A lot of interest has gone out to particles with tetrahedrally arranged patches. Through simulations it has been found that under the right conditions these particles self-assemble into a diamond crystal[3, 11]. The reason for the interest in the diamond crystal structure is that its properties are such that it is the best photonic crystal known so far[6] .

An extension to the basic patchy particle model is the introduction of patch specificity. In this case the patches cannot form bonds with all other patches, but instead can only connect with certain specific patches on the other particles. Increasing the patch specificity could also further direct crystallization into a desired crystal structure. Furthermore it could also lead to a better understanding of the behaviour of proteins, whose attractions are also sometimes highly specific.

Being able to design patchy colloids that are able to self-assemble into a desired crystal structure would have many applications. For this a very good knowledge of the behaviour of patchy particles is required. In this thesis one such patchy particle system is examined. More specifically the equilibrium behaviour of particles whose patches are arranged in an octahedral fashion are studied. The patches in this model are highly patch-specific, i.e. each patch on a particle can only be attracted to a single specific patch on other particles. This study is done through computer simulations.

Outline In section 2 the patchy particle model that is examined in this thesis will be explained in detail. Creating the simulation environment for this particle model however has to be built in steps. In section 3 the simulation techniques and theory behind the model are explained. Then in the section 4 the results of the simulations on the octahedral patchy particle model are discussed. Finally in section 5 a summary of the results are given along with a few final remarks.

2 The Model

In this thesis, a "patchy" particle model is studied in which the colloids are modelled as hard spheres which are decorated with attractive patches. The patchy particles are arranged in an octahedral arrangement. This particle model is an application of the model introduced by Kern and Frenkel[5]. The attraction between the patches are modelled as a square well potential. The particles cannot overlap each other due to their hard core potential $\Phi_{HS}(r)$, which is given as follows:

$$\Phi_{HS}(r) = \begin{cases} \infty & r < \sigma \\ 0 & r \geq \sigma \end{cases} \tag{1}$$

where r is the distance between the two particles and σ is the particle diameter.

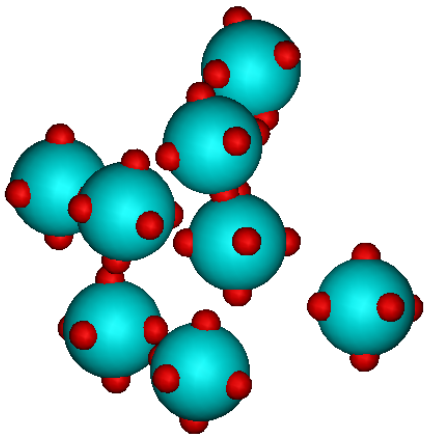

Figure 1: Octahedral patchy particles arranged in a simple cubic crystal. The particles (blue) are decorated with patches (red) which are bonded with one another.

The patches can only form bonds if they are within a certain distance δ from each other and if their angle with respect to each other is not too large. In most studies of patchy colloidal particles the patches have no specificity, i.e. every patch on particle i can form a bond with any of the patches on particle j. For the purpose of this thesis, this interaction type will be referred to as a patch-patch interaction. It is also possible, however, to introduce specificity to the interactions between patches. In the model studied in this thesis each patch on particle i can only interact with a single specific patch on particle j. This interaction type shall be referred to as a patch-antipatch interaction. The patch-antipatch interaction potential between two particles i and j is given by:

$$u_{patch}(i,j) = u_{sw}(r_{ij}) \sum_{\alpha,\beta=1}^{6} \delta(\alpha,\beta)\phi(r_{ij},\hat{p}_i^{\alpha})\phi(r_{ji},\hat{p}_j^{\beta}) \tag{2}$$

where $u_{sw}(r_{ij})$ is a square well potential that equals ϵ, the interaction strength between two patches, if the distance between particles r_{ij} is less than the cut-off range δ. In most of this paper the interaction strength ϵ will be set to one. The function $\delta(\alpha,\beta)$ equals one if patch α interacts with patch β, and zero otherwise. The function $\phi(\vec{r}_{ij},\hat{p}_i^{\alpha})$ is defined as follows:

$$\phi(\vec{r},\vec{p}) = \begin{cases} 1 & \hat{r}\cdot\hat{p} > \cos\theta_m \\ 0 & else \end{cases} \tag{3}$$

In this equation θ_m is the largest angle possible for a patch to still be able to connect to patches on other particles.

For the simulations in this paper, the cutoff range is chosen to equal $\delta = 1.24\sigma$ and the maximum patch interaction angle is chosen to equal $\cos\theta_m = 0.94$. When using these values a patch cannot simultaneously form bonds with multiple other patches and particles can only bond with one another through a single bond.

In the rest of this paper, often reduced units are used. The temperature is denoted by $T^* = K_bT$, the density by $\rho^* = \rho\sigma^3$, the pressure by $p^* = \beta p\sigma^3$ and the chemical potential is denoted by $\mu^* = \beta\mu$

3 Methods and Theory

3.1 Monte Carlo Simulations

All the simulations in this paper have been run using *Monte Carlo* simulation techniques. More specifically they rely on applications of the *Metropolis algorithm*. Therefore a brief explanation of this algorithm is in order.

A Monte Carlo method is most generally a computational method for solving a problem by generating a number of suitable samples according to a specific distribution. It is a very general scheme that has applications in many fields of science.

The Metropolis algorithm is a type of Monte Carlo method, often used in statistical physics. It relies on creating a sequence of samples according to a specific probability distribution. Starting from an initial state x, the algorithm randomly chooses a next state x' according to a given probability distribution. The probability for reaching state x' shall be denoted by $P(x \to x')$. There are two conditions which any Metropolis algorithm must adhere to, namely *balance* and *ergodicity*. However, since balance is often a difficult condition to ensure, usually *detailed balance* is proven instead, which is a stronger condition and guarantees balance.

Detailed balance is the condition that the probability of the system being in a state x and then reaching state x' must be equal to the probability of the system being in a state x' and then reaching state x. This can be written compactly as:

$$P(x)\,P(x \to x') = P(x')\,P(x' \to x) \tag{4}$$

Ergodicity is a property that is ensured when any possible state can be reached from any other state within a finite number of steps. In short:

$$P(x \to x') > 0 \qquad \forall\, x,\, x' \tag{5}$$

An often used technique in the Metropolis algorithm is that when in a given state a next trial state is randomly chosen. This trial state can then be accepted or rejected according to a desired probability distribution. In the case of particle simulations the probability distribution is the Boltzmann distribution. For these simulations the acceptance probability must depend on the Boltzmann factors of the initial and trial state. By choosing as an acceptance probability their relative Boltzmann weight, which depends on

the difference in energy dE between the initial and trial state, the resulting system will have a Boltzmann distribution. Therefore the probability of accepting the trial state equals:

$$P(dE) = e^{-\beta\, dE} \tag{6}$$

3.2 NVT Algorithm

Creating a working model as described above has been achieved in several steps. The first step is simulating an NVT ensemble using C++. In an NVT ensemble the number of particles N, the volume V and the temperature T are fixed. Since the particles in the model studied in the paper have a hard core potential, this potential for particles is also adopted in the NVT simulations.

In the simulations a box of volume $V = x \times y \times z$ is filled with hard-sphere particles, as can be seen in figure 2. These particles then undergo random displacements using a Monte Carlo algorithm. The algorithm works as follows:

1. Randomly choose one of the N random particle.
2. Randomly choose a small trial displacement $d\vec{r}$ of the particle in three dimensions. The displacement in each dimension is chosen from a uniform distribution in the range $[-dr_{max}, dr_{max}]$.
3. Accept or reject the trial displacement according to the following condition:
   (a) If the particle overlaps with another particle, reject the displacement.
   (b) Else accept the trial displacement..

By repeating this algorithm many times the simulation will correctly sample the configurations available to the NVT system. It is clear that the acceptance probability of this algorithm is the relative Boltzmann distribution as defined in formula 6.

The boundary conditions of this system are chosen to be periodic, i.e. when a particle passes one of the edges of the box it returns at the other side. By imposing periodic boundary conditions particles near the edge of the box are close to particles on the opposing edge. It is as if an additional

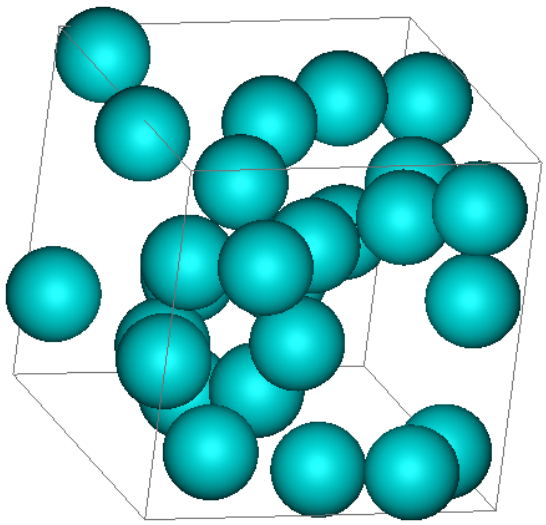

Figure 2: Hard sphere particles in a box

system is placed on each of the edges of the system. Periodic boundary conditions therefore are a good candidate for observing the behaviour of a many-particle system, even though the system itself might not have many particles.

In this algorithm the duration of the simulation is measured in cycles. One cycle equals a total of N repetitions of the trial displacement algorithm. A cycle therefore scales with the number of particles such that on average in one cycle each particle will have made one trial displacement. Note that this does not necessarily mean that each particle will have indeed made a trial displacement.

The initial behaviour of the system will depend on the initial configuration of all the particles. If they are randomly placed all over the box they will certainly move differently than if they are neatly stacked in an ordered crystal structure. There are cases when the initial configuration plays a crucial role in the total behaviour of the system, not just its initial behaviour, but this will be discussed later. What is of importance now is that we are interested in the equilibrium properties of the system. Therefore it is necessary for the system to be properly thermalized before starting measurements,which can be achieved by running a number of initial cycles.

Another point of interest is the trial displacement. A random particle is chosen and displace by an amount $d\vec{r}$. The average probability of a trial displacement being accepted will decrease if the maximum displacement dr_{max} is larger. This will be especially true if the density of the system is high. On the other hand if the average displacement is too low, the particles will move slowly and it will therefore take a long simulation time before enough useful data can be gathered. Therefore it is important to choose a right value of dr_{max} that is neither too high nor too low. As a rule of thumb a displacement acceptance ratio of about one-third is a good probability. Adjusting dr_{max} such that the acceptance ratio is roughly one-third will speed up the simulations considerably. In the simulations in this thesis the value of dr_{max} is constantly changed during thermalization to adhere to the rule of thumb. This is done by implementing a check after every cycle to see if the number of accepted displacements is roughly one-third. If this is not the case, dr_{max} is changed accordingly. The value of dr_{max} should not be changed during actual measurement simulations. The reason is that detailed balance, a condition required for correct use of the Metropolis algorithm, is not preserved during a change of dr_{max}. This is not a worry during thermalization, since the only goal is to properly thermalize the system before measurements. However a variable dr_{max} during measurements may lead to incorrect data. Instead, the optimal value of dr_{max} right after thermalization is used during the entire measuremt simulation.

3.3 NPT Algorithm

An NPT ensemble is an ensemble in which the number of particles N, the pressure p and the temperature T are fixed. Since the pressure p is fixed instead of the volume V, as is the case in the NVT system, the volume is free to change. It will do so until it has reached its equilibrium volume, around which it will still fluctuate. Hence in an NPT simulation there are two types of trial moves, namely (i) trial discplacement attempts as described in section 3.2; and (ii) trial volume changes. The algorithm for the trial volume changes can be described as follows:

1. Choose a volume V_{new} which differs slightly from the old volume V_{old}. The volume difference is chosen uniformly in the range $[-dV_{max}, dV_{max}]$ and all dimensions are scaled by the same factor.

2. Reject the volume change with a probability P, which equals:

$$P = min\{1,\, e^{-p(V_{new}-V_{old})} \times (\frac{V_{new}}{V_{old}})^N\} \tag{7}$$

3. If the volume change is not rejected, move all the particles such that their positions scale with the change in volume

4. Check if the particles overlap each other

5. If none of the particles overlap each other, accept the attempted volume change, else move all the particles back to their original positions

There are two checks in the algorithm above which both have to be accepted for the trial volume change to be accepted. The first check is a probability check and is done at step 2 in the algorithm. The second check is a particle overlap check and is done at step 4 in the algorithm. It is possible to change the order of the two checks, but since the first check is performed during every attempted volume change, whereas the second check is only performed if the first check is passed, choosing the check that requires the least calculations as the first check is a wise choice. The probability check is much less computationally intensive than the particle overlap check, and therefore placing the probability check first is clearly the better option. Another thing to notice about the volume changes is that particles can only overlap each other if the new volume V_{new} is smaller than the old volume V_{old}. Therefore the second check is only required in these cases, which can save a considerable amount of calculations.

Since there are now two types of MC moves, namely a trial displacement attempt and a trial volume change attempt, a question that must be addressed is how frequently each of the two moves should be performed. A thing to note is that a volume change attempt requires many more computations, since it loops checks for overlaps between all the particles, whereas a displacement attempt checks for overlaps for a single particle. If both algorithms were to be applied equally, between two volume change attempts only a single particle would have undergone a displacement attempt. The system would have barely changed. This would be rather inefficient. On the other hand, if a volume change attempt is used very rarely, the volume of the system will vary very slowly, resulting in a long simulation time before enough useful information can be gathered. Therefore a good balance is needed.

In the simulations in this paper a volume change attempt is performed on average once per cycle.

The volume change attempts also have an acceptance ratio which depend on both checks and can be modified by changing the range in which the new volume V_{new} can differ from the old volume V_{old}. A larger volume change usually results in a smaller acceptance ratio. In the simulations I have chosen a volume V_{new} which differs by no more than dV_{max} from V_{old} and has a uniform probability in that volume range. During thermalization the value of dV_{max} is constantly changed such that the acceptance ratio stays at roughly 10% .

It is clear that for both of the algorithms the bottleneck of the code is checking for overlaps between particles. For an attempt to displace a particle it is required to check if a single particle overlaps with any other particle, and for an attempt to change the volume a check has to be made for every particle if it overlaps with any other particle. The simplest way to check if a particle is overlapping with any other particle is to loop through all the other particles and compute their distance from the original particle. If any of the distances is smaller than the particle diameter σ, the two particles are overlapping each other. Since a single particle overlap check loops through N particles, for a displacement attempt this will result in a computation of $\mathcal{O}(N)$. For a volume change attempt one has to repeat this check for all of the N particles, this will results in a computation of $\mathcal{O}(N^2)$. These checks are very computationally intensive, and in fact there are faster checks for overlap. One improvement is by implementing cell lists.

3.3.1 Cell List

Cell lists are created by dividing the volume into cells with dimensions slightly larger than the range of the interaction, in this case σ. A list is maintained of all the cells and the particles whose centers are residing within them. The advantage of implementing a cell list is that whenever one has to check whether or not a particle is overlapping with any of the other particles, instead of checking for overlaps with all the other particles, only the particles residing in the cell of the particle and its neighbouring cells have to be checked. The working of a cell list is shown in figure 3, in which a particle overlap check for particle 1 is visualized. Each arrow indicates a check for overlap between the particles joined by the arrow. In the left image, the check is performed without use of a cell list. In this case all the other particles have to be

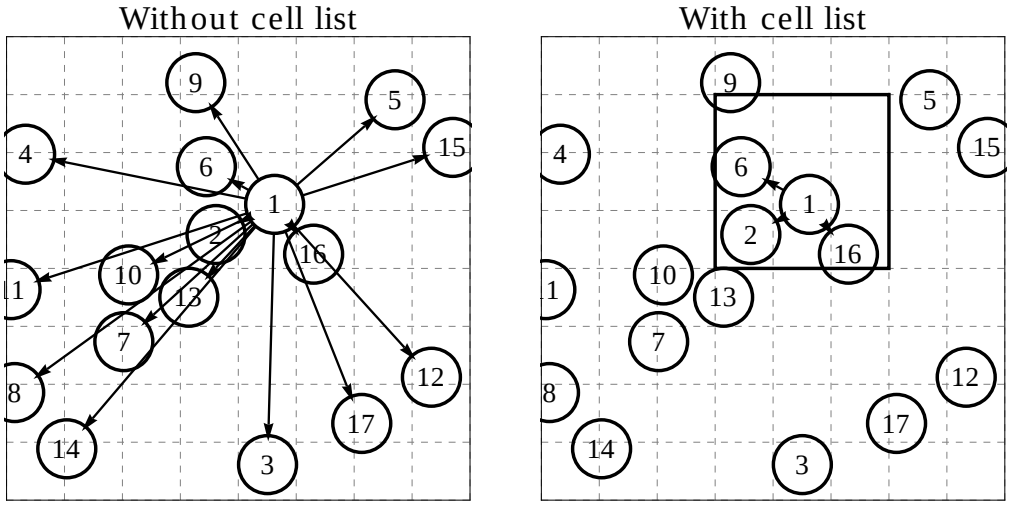

Figure 3: Visualization of a particle overlap check without a cell list (left) and with a cell list (right). Each arrow indicates a check for overlap between the particles joined by the arrow

checked. In the right image, the gridlines indicate the cells. By using cell lists, only particles whose centers reside in the cells neighbouring the cell of particle 1, indicated by the black rectangle. As one can see in the figure, the number of particles that have to be checked for overlap is reduced from 16 to 3. Comparing this to a system of a few hundred particles, one can easily see the advantage of introducing cell lists.

Implementing cell lists reduces checking for single particle overlapping to an $\mathcal{O}(1)$ computation and checking for overlaps between all particles to an $\mathcal{O}(N)$ computation. Therefore the added computations arising from maintaining and manipulating the cell list are easily made up for, especially when N is large.

3.3.2 NPT Results

Simulating the NPT ensemble as described above, it is possible to find the equation of state for a system of hard spheres, i.e. the relation between the pressure and the density of the system. This has been done for a total of $7 \times 7 \times 10$ particles. The particles are originally arranged on an fcc lattice

at a density high enough for the particles to initially remain in a crystal structure. After thermalization the system will either change into a fluid or else remain in an fcc structure, depending on the pressure.

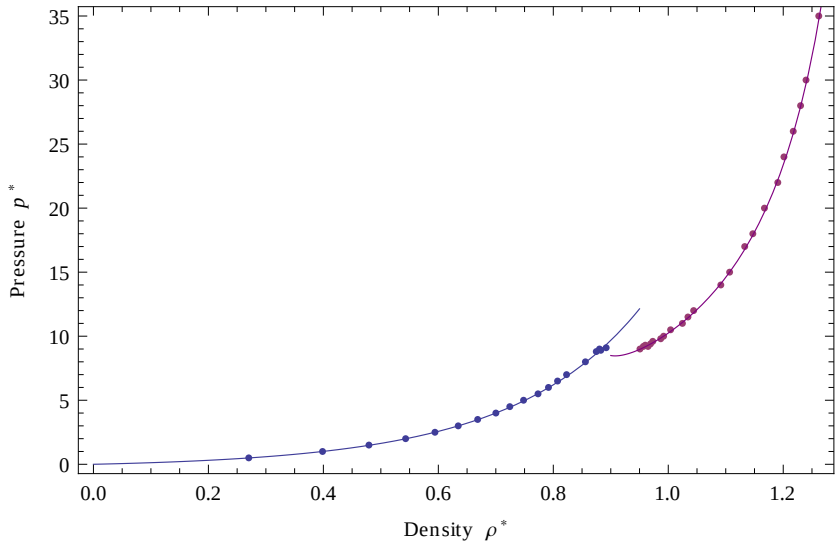

Figure 4: Equation of state results for the hard sphere system, together with the solid approximation by Speedy and the fluid approximation by Speedy (blue lines)[4]

The simulations have been run for a total of 200.000 cycles, half of which are used for thermalization. The results are shown in figure 4. As a comparison, approximations made by Speedy[4] for the fluid and solid equations of state have also been added to figure 4.

3.4 Free Energy Calculations

One property of particular interest is the free energy of the system. With knowledge of the free energy it is possible to determine the phase that is stable for a given pressure and temperature. Unfortunately the free energy of a system is not a directly measurable property, as it depends on the entropy. There are, however, techniques to obtain the free energy for a specific temperature and pressure.

An often used technique is thermodynamic integration. The technique works by starting from a reference system for which the free energy is known,

and then integrating along a reversible path to the system of interest. The reference system may be one for which the free energy has been calculated analytically, or it may have been found through previous simulations.

The two systems between which the integration is performed can differ in one or more thermodynamic variable, or their Hamiltonian may not be the same. In either case the integration is usually performed via simulations, by changing the parameters of the reference system in steps such that the end-result is the desired system.

If one of the thermodynamic variables is not the same for the two systems, integration can be performed along a path where one of the thermodynamic variables is kept constant, such as along an isotherm (constant temperature T). If at a reference system the free energy $F(\rho_0, T)$ is known, in the case of an isotherm the free energy of the end-system can be obtained by [13]:

$$\frac{\beta F(\rho, T)}{N} = \frac{\beta F(\rho_0, T)}{N} + \int_{\rho_0}^{\rho} \frac{\beta\, p(\rho')}{\rho'^2} d\rho' \tag{8}$$

A condition for thermodynamic integration to work is that the system does not undergo a first order phase transition during the changing of parameters. This means that for the NPT hard sphere system the free energy of the fluid and of the solid have to be calculated by seperate means.

3.4.1 Fluid Free Energy

Calculating the free energy for the hard sphere fluid can be done by using an ideal gas reference system. By starting from a very low density system, the average distance between particles is very large, causing the particles to hardly interact with each other, effectively becoming an ideal gas. By slowly increasing the density and integrating the difference in free energy it is possible to obtain the free energy for the whole fluid line of the hard sphere system. By keeping the temperature T of the system constant the thermodynamic integration can be done along an isotherm, and one can use equation 8. The free energy of the ideal gas system $F_{id}(\rho)$ has been calculated [4, p. 256][13]:

$$\frac{\beta F_{id}(\rho)}{N} = \log\left(\rho\Lambda^3\right) - 1 + \frac{\log\left(2\pi N\right)}{2N}. \tag{9}$$

For convenience the value of the thermal de Broglie wavelength is set to $\Lambda = \sigma$ such that $\rho\Lambda^3$ is the dimensionless density.

The following formula gives the free energy of the fluid hard sphere system at a specific density:

$$\frac{\beta F(\rho, T)}{N} = \frac{\beta F_{id}(\rho)}{N} + \int_0^\rho \frac{\beta p(\rho') - \rho'}{\rho'^2} d\rho' \tag{10}$$

The second term in Eqn. 10 is the integration from the low density reference system to the system at density ρ. Since it depends on the pressure as a function of density the necessary information for the integration can be gathered from the fluid line in the equation of state. By using the equation of state and equations 9 and 10 the free energy for the complete fluid phase of the NPT hard sphere system can be determined.

3.4.2 Solid Free Energy

Calculating the free energy for the solid phase is more complicated than it is for the fluid phase. One technique that is often used for calculating the free energy of solids is the Einstein integration method. The reference system chosen is an Einstein crystal, a crystal in which every particle is bounded to its ideal lattice position by a harmonic potential, and does not interact with neighbours. The free energy has been calculated analytically for this system. The potential energy of the Einstein crystal depends on a spring constant α and looks as follows:

$$U_{harm} = \alpha \sum_{i=0}^{N} (\mathbf{r}_i - \mathbf{r}_{i,0})^2 \tag{11}$$

where $\mathbf{r}_i$ is the current position of particle i, and $\mathbf{r}_{i,0}$ is its original lattice site.

Instead of changing the density of the system in this case the potential energy function is modified. This is done by introducing a coupling parameter λ to the potential energy function such that when $\lambda = 1$, the potential energy function is that of the Einstein crystal U_{harm} and when $\lambda = 0$, the potential energy function is the potential energy function of the hard sphere U_{HS}, as defined in equation 1. The combined potential energy function looks as follows:

$$U(\lambda) = U_{HS} + \lambda U_{harm} \tag{12}$$

It seems logical that the hard sphere potential energy function U_{HS} should diminish when $\lambda = 1$ and should therefore also depend on λ. However, in an Einstein crystal the particles are assumed to not interact with each other. So if the spring constant α is chosen to be sufficiently high, a particle will hardly move and therefore practically never interact with neighbouring particles. Thus, by starting at a system in which $\lambda = 1$ by slowly lowering the coupling parameter λ, one finally arrives at the system of interest.

There are a few practical issues to consider. First of all, for the Einstein integration to work, the harmonic potential energy function must not exhibit periodic boundary conditions, i.e. when a particle whose ideal lattice position is close to the edge of the system jumps to the other side, the harmonic potential must treat the particle as though it is still residing at the original side of the lattice.

Another issue is that in the limit $\lambda \to 0$, even if the density is sufficiently high that the particles remain in a crystal structure, the crystal itself may start to drift. As a result, the mean-squared particle displacement $\langle \mathbf{r}^2 \rangle$ will exhibit a divergence at low λ. This problem can be circumvented by adding the constraint of having a fixed center of mass. If a particle is moved, all the other particles must move a small amount in the opposite direction such that the center of mass stays the same. Updating the positions of all the particles every time a particle has undergone a displacement is very costly. Luckily, it turns out that for the calculations in the simulation one only needs to keep track of the displacement of the center of mass $\Delta\mathbf{R}_{cm}$. Every time a particle undergoes a displacement $\Delta\mathbf{r}$, the center of mass shifts by an amount $\Delta\mathbf{R}_{cm} \to \Delta\mathbf{R}_{cm} + \Delta\mathbf{r}/N$.

Since every time a particle moves all the other particles move as well, All the particles contribute to the change in the harmonic potential energy. This would also seem like a costly calculation. However it turns out that this is not the case[4, p. 250]:

$$\begin{aligned}\Delta U_{harm}(\lambda) &= \lambda\,\alpha \sum_{j\neq i}^{N}\Big[(\Delta\mathbf{r}_j - \Delta\mathbf{r}_i)^2 - \Delta\mathbf{r}_j^2\Big] \\ &\quad + \lambda\,\alpha\Big[\big(\Delta\mathbf{r}_i + (1-1/N)\Delta\mathbf{r}_i/N\big)^2 - \Delta\mathbf{r}_i^2\Big] \\ &= \lambda\,\alpha\left(2\Delta\mathbf{r}_i\cdot\Delta\mathbf{r}_i/N + \frac{N-1}{N}(\Delta\mathbf{r}_i/N)^2\right)\end{aligned} \tag{13}$$

Adding a fixed center of mass constraint also changes the free energy of the system. This change in free energy can also be calculated analytically, both for the Einstein crystal and the non-Einstein crystal. Calculating the total free energy of the crystal can be accomplished by starting with the free energy of an Einstein crystal with fixed center of mass F_{ein}^{CM}, then use thermodynamic integration to calculate the difference in free energy between the constrained Einstein crystal F_{ein}^{CM} and the constrained non-Einstein crystal F^{CM}, which is given by: $\Delta F_{ein}^{CM} = F^{CM} - F_{ein}^{CM}$. The final step is to find the free energy of the unconstrained crystal F by calculating the free energy difference $\Delta F = F - F^{CM}$.

The free energy per particle of an Einstein crystal with fixed center of mass equals[4, 9]:

$$\frac{\beta\,F_{ein}^{CM}}{N} = -\frac{3}{2}\,log\left(\frac{\pi}{\alpha\beta}\right) - \frac{3}{2N}\,log\left(\frac{\alpha\beta}{\pi}\right) + \frac{log\,\rho}{N} - 2\frac{log\,N}{N} \tag{14}$$

The difference in free energy between the constrained Einstein crystal and the constrained non-Einstein crystal is obtained using thermodynamic integration. More specifically, by changing the value of the coupling constant λ from 0 to 1, and integrating along the path, the free energy difference ΔF_{ein}^{CM} can be found:

$$\frac{\beta\Delta F_{ein}^{CM}}{N} = \frac{\beta F^{CM}}{N} - \frac{F_{ein}^{CM}}{N} = -\int_0^1 d\lambda\,\big\langle U(\lambda)\big\rangle \tag{15}$$

This thermodynamic integration has to be performed via simulations at a fixed density. By choosing several points of λ between 0 and 1 it is possible to numerically integrate this equation. The question arises as to what are a good choice of points. It turns out that an excellent technique has already

been devised for calculating such integrals, the Gauss-Legendre Quadrature method[10]. For a given number n, the Gauss-Legendre Quadrature method chooses n values of λ, which shall be referred to as λ_i and further chooses for each λ_i an appropriate weight w_i. The integral can then be approximated by the following calculation:

$$\int_0^1 d\lambda \left\langle U(\lambda) \right\rangle \approx \sum_{i=1}^{n} \left\langle U(\lambda_i) \right\rangle \cdot w_i \tag{16}$$

This technique works especially well for smooth functions, providing a very accurate estimate. The potential energy is expected to behave quite smoothly, as the harmonic potentials are gradually turned on, and so the Gauss-Legendre Quadrature method seems a good choice.

The free energy difference ΔF between the constrained crystal F^{CM} and the unconstrained crystal F equals[4, 9]:

$$\frac{\beta \Delta F}{N} = \frac{\beta F}{N} - \frac{\beta F^{CM}}{N} = \frac{log\rho}{N} - \frac{d}{2N} log\big(\frac{\beta\alpha}{\pi}\big) \tag{17}$$

Combining equations 14, 15 and 17, the total free energy per particle of the unconstrained crystal is given by:

$$\frac{\beta F}{N} = \frac{\beta F_{ein}^{CM}}{N} + \frac{\beta \Delta F_{ein}^{CM}}{N} + \frac{\beta \Delta F}{N} \tag{18}$$

$$= -\tfrac{3}{2} log\big(\tfrac{2\pi}{\lambda}\big) - \tfrac{3}{2N} log\big(\tfrac{\lambda}{2\pi}\big) + \tfrac{log\,\rho}{N} - 2\tfrac{log\,N}{N} - \tag{19}$$

$$- \int_0^1 d\lambda \big\langle U(\lambda) \big\rangle + \tfrac{log\,\rho}{N} - \tfrac{d}{2N} log\big(\tfrac{\beta\,\alpha}{\pi}\big) \tag{20}$$

Often the quantity of interest is not the free energy F of the system but the excess free energy F^{ex} over the ideal gas free energy F^{id}, as given in equation 9. The Excess free energy per particle then equals:

$$\frac{\beta F^{ex}}{N} = \frac{\beta F}{N} - \frac{\beta F^{id}}{N} = \frac{\beta F}{N} - log\,\rho + 1 - \frac{log(2\pi N)}{2N} \tag{21}$$

According to Poisson et al.[9] the leading finite size corrections for a system of hard spheres is $logN/N$ dependent. Taking this term into account will lead to a better estimate for the free energy of an infinite hard sphere

system, as it gives a correction for the difference in free energy due to having a finite system.

Once again, when the free energy at a specific density is known for the crystal phase, by keeping the temperature constant and integrating along the isotherm as given by equation 8, the free energies for the other densities of the crystal phase can be calculated as well.

3.4.3 Results

As a check for the simulations, the free energy of the hard sphere system has been calculated for the solid phase at a density of $\rho^* = 1.0409$, slightly above the coexistence density region.

The Monte Carlo simulations have been run for a total of 600.000 cycles, a third of which were run for thermalization. for a system of $8 \times 8 \times 12 = 768$ particles, initially arranged in an fcc structure.

By using equations 20 and 21, along with the leading finite size correction, a free energy of $\frac{\beta F}{N} = 4.9529\, k_b T$ was found with an excess free energy equalling $\frac{\beta F^{ex}}{N} = 5.9116\, k_b T$.

This has been compared to the value as obtained by Poisson et al.[9] who determined the excess free energy value to be $\frac{\beta F^{ex}}{N} = 5.9111\, k_b T$ for a system of 768 particles. The difference in free energy equals $\Delta F = 0.005\, k_b T$. This gives a strong indication that the simulations are working correctly.

3.4.4 Coexistence Point

With knowledge of the free energy of the system, it is possible to find the coexistence region of the system, i.e. the density region where the solid phase and liquid phase both exist. Two phases are in coexistence if their temperatures T, their chemical potentials μ and their pressures p are equal. There are several techniques for finding the point of coexistence, and the technique described here is called the common tangent method.

The chemical potential μ is defined as:

$$\mu = \frac{G}{N} = \frac{F + pV}{N} = f + \frac{pV}{N} \tag{22}$$

where G is the Gibbs free energy and f is the Helmholtz free energy per particle. As we know the free energy F of both phases through thermodynamic integration and through the equation of state, we know the chemical

potential of the hard sphere system. If we find the densities of the liquid and solid phase where the chemical potentials and the pressures are equal, we know the point of coexistence.

One way to find the two points where the chemical potentials and pressures are equal is to plot a graph of $f \cdot \rho$ as a function of the density ρ for both the solid and liquid phase. The common tangent of the two free energy functions connects the two points where the chemical potentials and the pressures of the two systems are equal. This is a rather straightforward technique, and the reason the points connected by the common tangent have equal chemical potentials can be shown quite easily.

The differential of the free energy is given by $dF = -pdV - SdT + \mu dN$ for a one-component system. It follows that:

$$\left(\frac{dF}{dV}\right)_{T,N} = -p \tag{23}$$

On the other hand:

$$\left(\frac{dF}{d\rho}\right)_{T,N} = -\frac{V^2}{N}\left(\frac{dF}{dV}\right)_{T,N} \Rightarrow \left(\frac{dF}{dV}\right)_{T,N} = -\frac{N}{\rho^2}\left(\frac{dF}{dV}\right)_{T,N} \tag{24}$$

Combination of equations 23 and 24 leads to:

$$\left(\frac{dF}{d\rho}\right)_{T,N} = \frac{pN}{\rho^2} \Rightarrow \left(\frac{df}{d\rho}\right)_{T,N} = \frac{p}{\rho^2} \tag{25}$$

From this it follows that:

$$\left(\frac{d(f \cdot \rho)}{d\rho}\right)_{T,N} = \frac{p}{\rho} + f = \mu \tag{26}$$

So from this we can clearly see that the derivative of $f \cdot \rho$ with respect to ρ is simply the chemical potential. Two points connected by a common tangent have per definition the same derivative, so their chemical potential must be equal. From equation 26 it can also be shown that the pressures at the two points are equal. Define by ρ_1, f_1, p_1 the density, free energy per particle and pressure of the system at points one, and similarly let ρ_2, f_2, p_2 be the density, free energy per particle and pressure at point two. Then equation 26 states that:

$$\frac{p_1}{\rho_1} + f_1 = \frac{p_2}{\rho_2} + f_2 = \mu \tag{27}$$

With a little bit of rewriting we find:

$$p_1 + \rho_1(f_1 - \mu) = p_2 + \rho_2(f_2 - \mu) \tag{28}$$

$$p_1 + \big(\rho_1 f_1 + \mu(\rho_2 - \rho_1)\big) - \rho_2 f_2 = p_2 \tag{29}$$

The final step to notice is that $\rho_1 f_1 + \mu(\rho_2 - \rho_1)$ is equals to $\rho_2 f_2$, since μ is the slope of the common tangent. Therefore the two factors cancel each other out and we are left with: $p_1 = p_2$.

Another interesting point to note is that both the chemical potential and the pressure of the point of coexistence can be gathered directly from the formula for the common tangent. The common tangent is a straight line, so its formula has the form $a\rho + b$. We have seen earlier that the slope of the common tangent equals μ, so it follows that $a = \mu$. For the value of b, note that at any of the two points, say point 1, we have that $\rho_1 f_1 = \rho_1 \mu + b \Rightarrow b = \rho_1(f_1 - \mu)$. Comparing this to equation 26 we see that b is simply the pressure p. We conclude that the common tangent is given by the formula $\mu\rho + p$.

We have shown that the points of the two functions connected by the common tangent are indeed the points where both the chemical potentials and the pressures are equal, and so from the common tangent construction the region of coexistence can be determined.

To examine this method the common tangent method has been applied to the hard sphere data. First a fifth order polynomial was fitted for the data of the equation of state for both the fluid and solid phase. For the fluid phase however, the variables up to the quadratic term are known. First of all the hard sphere system approaches an ideal gas at low pressures, and the density of the ideal gas diminishes with zero pressure, it can be concluded that there is no constant term in the polynomial. Furthemore the monic term equals one, since it is the ideal gas contribution, which scales linearly with the density. Finally, since there is no constant term, and the monic term is effectively cancelled out through thermodynamic integration by equation 10, the quadratic term is the lowest order term in the integration, and so the value of the integrand is very sensitive to the value of the quadratic term. Its term can be calculated analytically and is called the (reduced)

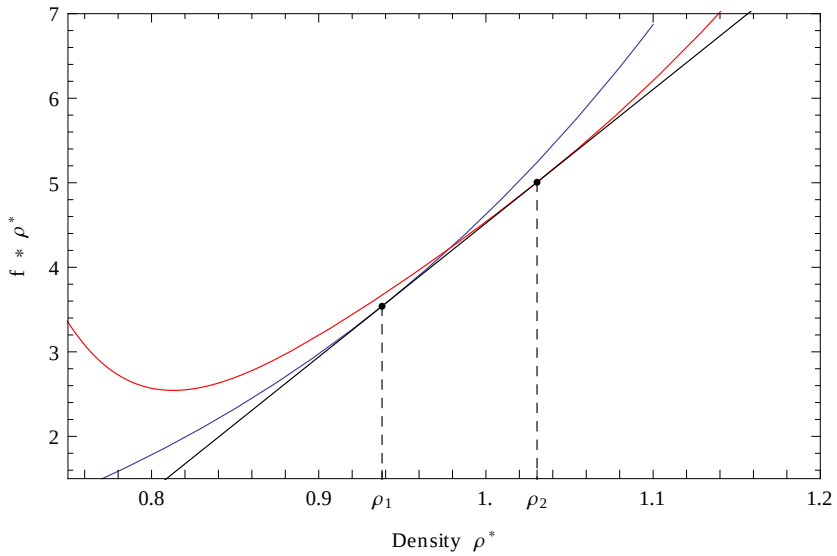

Figure 5: Common tangent for the hard sphere system (black line), along with fluid line (blue) and solid line (red). In the graph $f = \frac{\beta F}{N}$ is the free energy per particle. The coexistence densities ρ_1 and ρ_2 were found to equal $\rho_1 = 0.938$ and $\rho_2 = 1.031$.

second virial coefficient $B_2 = 2\pi$. Correctly fixing the first three terms in the fifth order polynomial will likely lead to a more accurate result. For the solid reference free energy the value was used which was found above using Einstein integration at a density $\rho^* = 1.0409$.

The results can be seen in figure 5. The common tangent touches the fluid line at a density $\rho_1 = 0.938$ and the solid line at $\rho_2 = 1.031$. Comparing this to the results from Noya, Vega and de Miguel[7] where the densities of coexistence were found to be equal to $\rho_1 = 0.9375(14)$ and $\rho_2 = 1.0369(13)$, we see that the data coincides nicely. The systems have different number of particles, and so finite size effects quite possibly account for the deviation in the values.

The coexistence pressure p^* and chemical potential μ^* have also been found from the common tangent and equal $p^* = 11.297$ and $\mu^* = 15.819$. This again seems in good agreement with the results from Noya, Vega and de Miguel [7], where the pressure was found to equal $p^* = 11.54(4)$ and the results from de Miguel [2], where a chemical potential of $\mu^* = 15.833(14)$ for

a system of 500 particles.

3.5 Adding Orientation

Now that the initial hard sphere model has been created and tested, the next step is to add patches and patch interactions to the particles. The interactions between the patches as described in section 2 will be adopted here. Since a patch is at a fixed position relative to its particle, a rotational degree of freedom has to be added. Particles therefore have to be able to rotate.

In the initial system configuration, the patches are placed at specific coordinates relative to their corresponding particles. In order to incorporate this rotational degree of freedom, a third trial attempt is included, namely a rotation attempt. In this rotation attempt a randomly chosen particle undergoes a trial rotation by a small randomly chosen angle $d\theta$. To simplify matters, the angle $d\theta$ is chosen along one of the three axes and is chosen uniformly in the range $[-d\theta_{max}, d\theta_{max}]$ for some defined $d\theta_{max}$. By rotating each of the patches on the particle by $d\theta$, the particle itself will have effectively undergone a rotation under the same angle.

The acceptance probability P of the rotation attempt depends on the difference in energy dE of the system due to rotation of the particle and is given by equation 6. Instead of looking at the free energies of the system as a whole before and after the rotation, a better option is to look at the number of bonds the patches of particle i make before and after the rotation. The change in free energy dE is then simply the difference in number of bonds multiplied by the well depth ϵ.

As bonds can also be created and broken during particle displacements and volume changes, the change in energy also has to be taken into account during these trial attempts. Therefore the acceptance probability criterion as given by equation 6 also has to be included.

For the simulations a rotation attempt is performed after every displacement attempt, such that on average one cycle constitutes N displacement attempts, N rotation attempts and 1 volume change attempt.

3.6 Stable Crystal Structures

For particles with patches it is not necessarily obvious what structures might be stable. The fcc structure which was the most favourable solid structure for

the hard sphere system seems less likely, as not all patches on the particles can form bonds with neighbours. The simple cubic structure however is an obvious candidate, as the patches are arranged in an octahedral fashion, making it easy to form a simple cubic structure. The downside of the simple cubic structure is that its packing fraction is ≈ 0.52, which is quite low. The structure is shown in figure 6.

A second likely structure is the body centered cubic (bcc) structure. Unfortunately the patches on a particle cannot form bonds with all its nearest neighbours. However, it can form the maximum number of bonds with its second-nearest neighbours. the minimum distance from its second-nearest neighbours equals $1.1225\,\sigma$, which is within the cut-off range δ. Since the bcc crystal has a higher packing fraction than the simple cubic crystal, namely ≈ 0.68, it is expected that especially at higher pressures this will be the stable state. The crystal structure is shown in figure 7

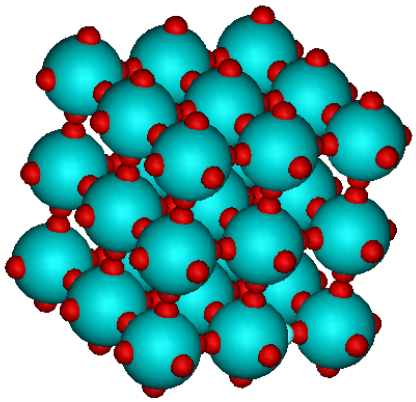

Figure 6: Octahedral patchy particles arranged on a simple cubic (sc) lattice.

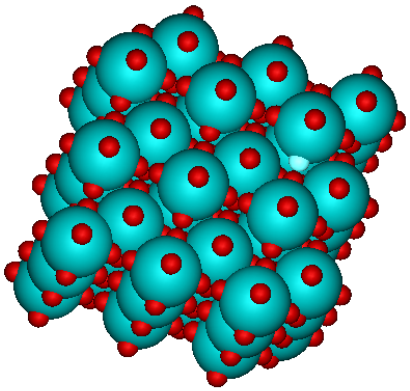

Figure 7: Octahedral patchy particles arranged on a body-centered-cubic (bcc) lattice.

3.6.1 Patchy NPT Results

As a check for consistency I have created an equation of state in the fluid region for patchy particles under the same simulation conditions as were

done by my supervisor Laura Filion for one of her previous projects. The simulation conditions are such that the particles each have four patches arranged in a tetrahedral fashion. Both the patch-patch configuration and the patch-antipatch configuration have been tested. Furthermore the simulations were run at a temperature $T^* = 0.2$ and the number of particles in this system equals $N = 6 \times 6 \times 10 = 360$. For the patch-patch case 600.000 MC cycles were performed, a third of which for thermalization, whilst for the patch-antipatch case 400.000 MC cycles were performed, half of which for thermalization.

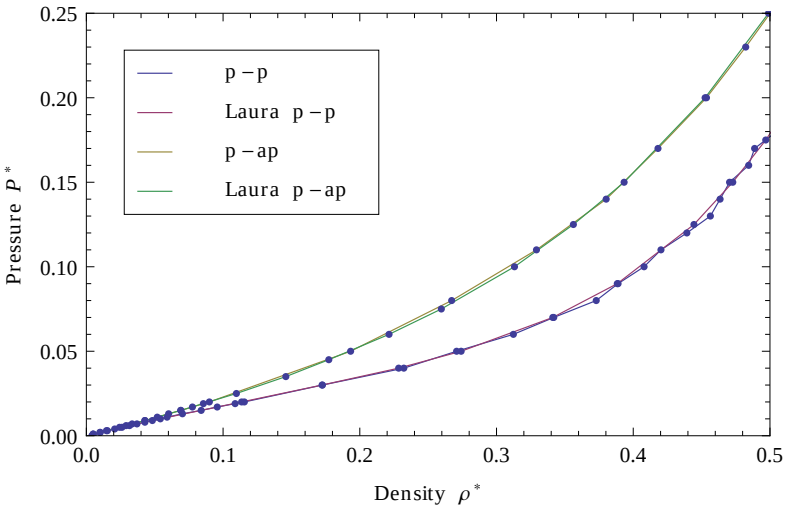

Figure 8: Fluid equation of state for tetrahedral patchy particles along with equation of state from Laura Filion's data

The results are shown in figure 8. The results seem to coincide very well. The results are more noisy for the patch-patch case at higher densities. This can be expected, since at higher densities equilibration usually takes longer. The data seems to coincide well enough to conclude that the program is working correctly.

3.6.2 Fluid Free Energy

For the fluid phase of the patchy particles the free energy can be calculated in exactly the same way as done for the hard sphere case, namely through thermodynamic integration along an isotherm from the reference ideal gas

system. By fitting a polynomial through the equation of state, the free energy can be determined for the complete fluid phase using equation 10. Once again the accuracy of the free energy calculation depends strongly on the value of the quadratic term in the polynomial fit, whose exact value is the reduced second virial coefficient B_2/B_2^{HS}, where $B_2^{HS} = (2/3)\pi\sigma^3$ is the second virial coefficient for the hard sphere system. As shown by Kern and Frenkel [5], the reduced second virial coefficient for a patchy particle system equals:

$$\frac{B_2}{B_2^{HS}} = 1 - \chi^2\big[(1+\delta/\sigma)^3 - 1\big](e^{\beta\varepsilon} - 1) \tag{30}$$

In this formula χ is the surface coverage of the attractive patches, which for the patch-antipatch case is given by:

$$\chi = \sqrt{N_p}\left(1 - \frac{1}{2}\cos(\theta_m)\right) \tag{31}$$

where N_p is the number of patches on a particle.

3.6.3 Solid Free Energy

For the free energy of the solid phase of the patchy particle system an Einstein crystal can be used yet again as a reference system. However in an Einstein crystal the particles do not have a rotational degree of freedom, and hence the rotational degree of freedom has to be incorporated into the thermodynamic integration scheme. This can be achieved by adding an additional potential to the system which ties the rotation of the particles. For this a harmonic rotational potential is applied to the particles that is similar to the harmonic springs connecting the particles to their lattice positions. This harmonic rotational potential U_{rot} is calculated by choosing two patches α and β on every particle, with unit vectors p^α and p^β, pointing from the center of the particle to the corresponding patch. The unit vectors p^α and p^β must not be scalar multiples of each other. The vectors $p^{\alpha,0}$ and $p^{\beta,0}$ are the initial directions of the two vectors, and further define $c_\alpha = p^{\alpha,0}\cdot p^\alpha$ and $c_\beta = p^{\beta,0}\cdot p^\beta$. The rotational harmonic potential is then defined as follows:

$$U_{rot} = \alpha\sum_{i=1}^{N}(2 - sign(c_\alpha)c_\alpha^2 - sign(c_\beta)c_\beta^2) \tag{32}$$

Here α is yet again the (harmonic) spring constant. Furthermore the potential U_{patch} is the potential due to the interactions between patches. The total potential again depends on λ and is given by:

$$U(\lambda) = U_{HS} + \lambda U_{patch} + (1-\lambda)U_{harm} + (1-\lambda)U_{rot} \tag{33}$$

We see that if $\lambda = 0$, the patches do not interact with one another and the particles are bound by the full harmonic and rotational potential to their initial positions, in both translation and orientation. On the other hand, if $\lambda = 1$, the patch interactions are at a maximum, whilst the harmonic and rotational potentials do not contribute to the system.

For the noninteracting crystal, there is an added contribution to the free energy, due to rotations. This rotational free energy F_{rot} is given by the formula:

$$\frac{\beta F_{rot}}{N} = -log\left[\frac{\int d\Omega \exp\left(-\beta U_{rot}\right)}{\int d\Omega}\right] \tag{34}$$

The upper integral has been calculated using Monte Carlo simulations by starting with two vectors perpendicular to each other, as would be the case for two patches in an initial configuration. For each Monte Carlo cycle these two vectors are rotated by a uniform rotation matrix, and then the exponent in Eq. 34 is calculated. Note that by rotating the vectors by the same rotation matrix the angle between the two vectors remains constant, as is also the case with patches on a particle. An issue which makes it difficult to achieve an accurate estimate of the integral is that it is very strongly peaked due to the spring constant α in the negative exponent. Therefore a very large sample has to be averaged over to achieve an estimate. After 10^{11} MC cycles the rotational free energy has been estimated to equal $\frac{\beta F_{rot}}{N} = 17.0975(21)$.

3.6.4 Results

To test for correctness of the Einstein integration with patches simulations were again run that have already been performed by Laura Filion. In this case the patches on the particles were again tetrahedrally placed, and the particles were arranged on a diamond cubic lattice, at a density of $\rho^* = 0.45$. The results, along with the results from Laura's simulations, are shown in Figure 9. As can be seen the data coincides rather nicely, only deviating at very low λ. A possible explanation for the deviation is due to the low

λ	$<U_{patch}>$	$<U_{patch}^{Laura}>$	$<U_{harm}>$	$<U_{harm}^{Laura}>$	$<U_{rot}>$	$<U_{rot}^{Laura}>$
1.74512×10^{-7}	−13.7986	−13.8472	0.202305	0.0238907	0.0867082	0.0801869
1.00379×10^{-6}	−13.8475	−13.8475	0.0239216	0.0238487	0.0801881	0.0802484
2.90139×10^{-6}	−13.8476	−13.8486	0.0238686	0.0237779	0.0801636	0.0801033
6.87123×10^{-6}	−13.8481	−13.8487	0.0238672	0.0238958	0.0800361	0.0800533
0.000015351	−13.8476	−13.848	0.0237602	0.0237472	0.0798602	0.0798706
0.0000344008	−13.8483	−13.8491	0.0236464	0.0236669	0.0795262	0.0795851
0.0000796018	−13.8503	−13.8499	0.0233697	0.0234452	0.078643	0.0786071
0.000192069	−13.8529	−13.8524	0.0226367	0.022752	0.0765849	0.0766032
0.000481561	−13.8593	−13.8586	0.0213213	0.0213281	0.0717102	0.0716885
0.00123905	−13.8671	−13.8675	0.0192074	0.0192015	0.0612249	0.0612145
0.00321391	−13.8761	−13.8765	0.0162282	0.0162301	0.0435782	0.0435235
0.00823393	−13.8829	−13.8826	0.0120238	0.0120219	0.0239402	0.0239512
0.0203971	−13.8868	−13.8866	0.00721184	0.00721143	0.0105136	0.0105071
0.047842	−13.8884	−13.8884	0.00397084	0.00396812	0.00448647	0.0044877
0.104161	−13.8888	−13.8888	0.00202804	0.00202728	0.00205902	0.00205772
0.206705	−13.8889	−13.8889	0.00103428	0.00103356	0.00103645	0.00103785
0.367941	−13.8889	−13.8889	0.000581346	0.000581237	0.000582117	0.00058292
0.579592	−13.8889	−13.8889	0.000368886	0.000368977	0.000369761	0.00036964
0.799394	−13.8889	−13.8889	0.000267565	0.00026751	0.000268218	0.000268055
0.958196	−13.8889	−13.8889	0.000223151	0.000223187	0.000223569	0.000223543

Figure 9: Comparison between simulations and previous results from Laura Filion for tetrahedral patchy particles in a diamond cubic lattice at a density $\rho = 0.45$

density of the system and low value of λ. The particles are very weakly tied to their original position, making it easier for them to drift and form bonds with other particles, even though it might be less favourable from an energy perspective. The data on a whole seems to coincide rather nicely and thus it may be assumed that the program is working correctly.

4 Results

4.1 Equation of State

To study the behaviour of octahedral patchy particles, the equation of state has been obtained through simulations for a system of $6 \times 6 \times 10 = 360$ particles for a range of temperatures. Once formed, bonds between patches are hard to break, and so reaching equilibration can take a large number of cycles. Therefore at least 10^6 thermalization cycles were run and a minimum of $1.5 * 10^6$ cycles were used for measurements. For each temperature three types of initial configurations were simulated, namely a low density fluid phase, a high density cubic crystal phase and a high density bcc crystal

phase.

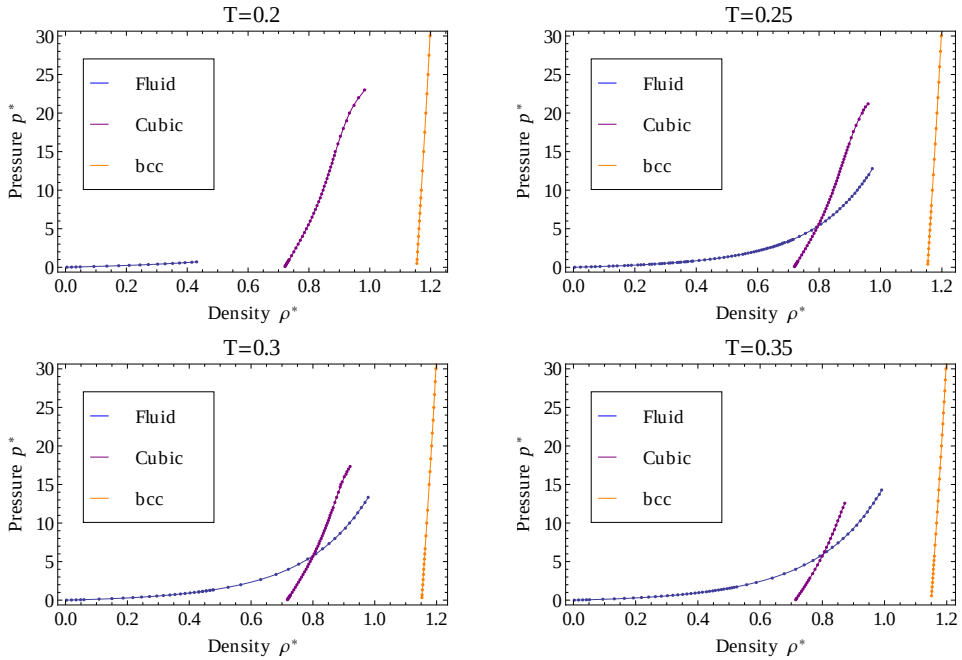

Figure 10: Equation of state for octahedral patchy particles for temperatures $T^* = 0.2$, 0.25, 0.3 and 0.35. Polynomial fits have been added to the figures.

In figure 10 the equations of state can be seen for temperatures ranging from $T^* = 0.2$ to $T^* = 0.35$. For the fluid and simple cubic phase the end of the equation of state represents the points where the phase transitions started to occur. The first thing to notice is that the crystal phases rarely transition into one another. This is more evident at lower temperatures. Although at a fixed pressure at most one of the two crystal structures can be the most thermodynamically stable phase, both structures seem to be stable depending on the initial configuration for a large range of pressures. This indicates that the crystal phases experience a lot of hysteresis because there is a large energy barrier to cross for a phase to transition into another more thermodynamically stable phase. This can be explained by the fact that for a phase transition from one crystal structure into another many bonds between patches have to be broken, requiring more energy at lower temperatures. On the other hand, at low temperatures the fluid phase only seems stable in a narrow range of pressures. This can be explained by the fact that in a fluid,

bonds are constantly formed and broken. For lower temperatures the energy gain due to a bond being formed is large, as is the cost in energy for a bond being be broken.

For the fluid phase at a temperature $T^* = 0.2$, the first phase transition is into the simple cubic crystal phase. At higher temperatures however, upon increase of the pressure, the fluid phase remains stable at higher densities than the simple cubic phase. At these temperatures the fluid phase experiences a phase transition into the bcc phase.

The simple cubic crystal phase also experiences phase transitions into the bcc crystal phase at high densities for low temperatures. At $T^* = 0.35$ however the simple cubic crystal phase first experiences a phase transition into the fluid phase and then into the bcc crystal phase. This indicates that at this temperature the fluid phase is more (meta)stable than the simple cubic phase at higher pressures.

For all temperatures, at higher pressures both the fluid phase and the simple cubic crystal phase seem to transition into the bcc crystal phase. This does not come as a surprise, since the bcc crystal phase has a much higher packing fraction than the simple cubic phase, and yet the particles can be oriented in such a way that all patches on all particles can be bonded simultaneously. At $T^* = 0.35$ however, at very low pressures the bcc crystal phase has been found to melt, indicating that the fluid phase is the stablephase at higher temperatures at low pressures.

In figure 11 the equation of state is shown at a temperature $T^* = 0.4$. At this temperature the simple cubic crystal phase has been found to be unstable at all pressures. At low pressures the simple cubic crystal phase melts quite quickly. The simple cubic crystal phase is therefore unstable at temperatures of $T^* = 0.4$ or higher. The bcc crystal phase has also been found to occasionally melt at lower pressures, from which one can conclude that the fluid phase is the stable phase at lower pressures. Furthermore at a pressure of roughly $p^* = 17$ both the fluid phase can be seen to experience a phase transition. This phase transition is in fact into the bcc phase, although a highly defective one.

It is clear from the equations of state that for temperatures above $T^* = 0.35$ The range in pressures in which the simple cubic crystal does not either melt or transition into the bcc crystal phase sharply decreases as the temperature increases. On the other hand at temperatures in the range $T^* = 0.2$ and below the two crystal phases seem very stable, whilst the fluid phase only seems to be stable at very low pressures. Therefore in the simulations

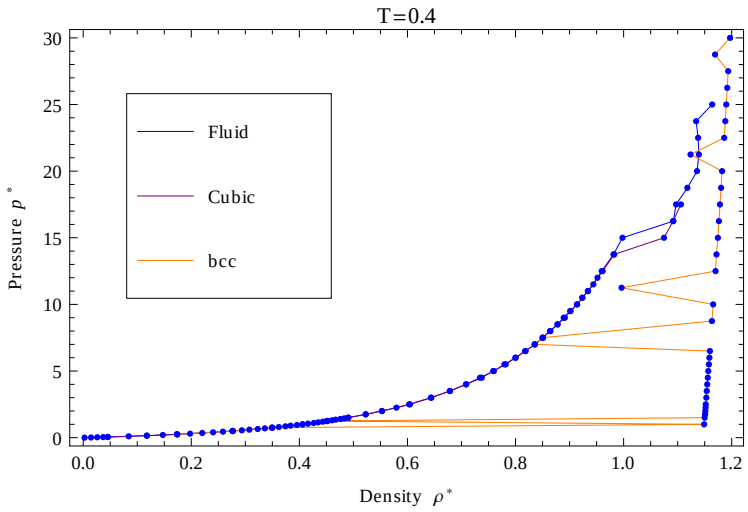

Figure 11: Equation of state for octahedral patchy particles at a temperature $T^* = 0.4$.

a temperatures have been chosen between $T^* = 0.2$ and $T^* = 0.35$ in steps of $\Delta T^* = 0.025$. The complete phase diagram in this temperature range will be discussed in section 4.4.

4.2 Fitting Polynomials Through the Equation of State

Through the equation of state data polynomials have been fitted. These can also be seen in figure 10. For the fluid phase the first three terms are known. The constant term must equal zero, as the fluid tends to the ideal gas in the zero pressure limit. The monic term equals 1, and the quadratic term is the second virial coefficient from equation 30. In figure 12 the fitted polynomial is shown for the fluid phase at a temperature $T^* = 0.25$. In the figure a dashed line is also shown, which is the fit up to the quadratic term, i.e. the second virial coefficient. As can be seen, the polynomial coincides nicely with the data points, even at low densities. This shows that the second virial coefficient from equation 30 is correct. This is an important conclusion, since the second term in the fitted polynomial plays an important role in the free energy calculations of the fluid phase, as discussed in section 3.4.4

For the two crystal phases a sixth degree polynomial is also fitted through the data. From figure 10 we can see that the fit coincides very well with the

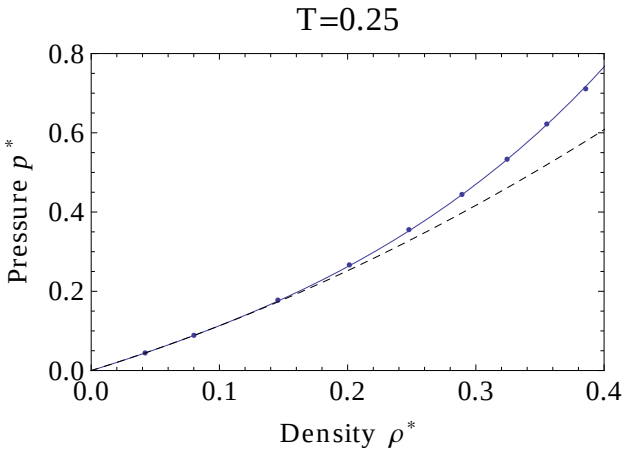

Figure 12: Sixth degree polynomial fit for the fluid phase at temperature $T^* = 0.25$. The dashed line indicates the polynomial up to the second virial coefficient B_2

data points.

4.3 Free Energy Calculations

The free energy of the fluid phase has been obtained through thermodynamic integration from the ideal gas reference state by using equation 10 along the equation of state.

For the simple cubic and bcc crystal phases Einstein integration has been performed to obtain the free energy. The intial configuration of the system is such that the particles are all fully bonded. A spring constant of $\alpha = 12000$ has been chosen. From trial simulations the shape of the average potential energy $\langle U \rangle_\lambda$ was found to be sharply peaked around $\lambda = 0$. Unfortunately the Gauss-Legendre Quadrature method did not provide an accurate estimate for the integral so instead for each temperature around 30 values of λ were chosen and the integral was obtained through interpolation. To achieve a more accurate result the logarithm of the data was interpolated and subsequently exponentiated back. In figure 13 the average potential energy per particle is shown as a function of λ for a temperature $T^* = 0.25$. Once the free energy has been calculated at a certain density, the free energy along the whole equation of state has been found through use of equation 8.

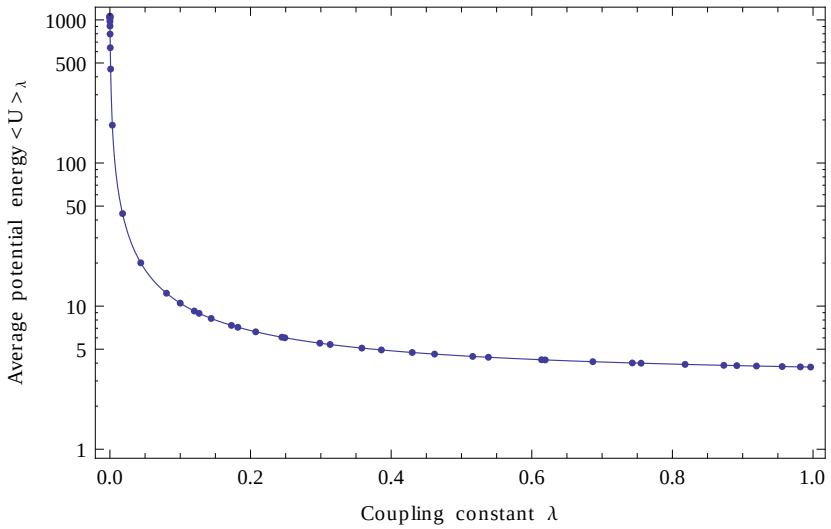

Figure 13: Average potential energy per particle $\langle U \rangle_\lambda$ as a function of λ at a temperature $T = 0.25$, along with the interpolated function.

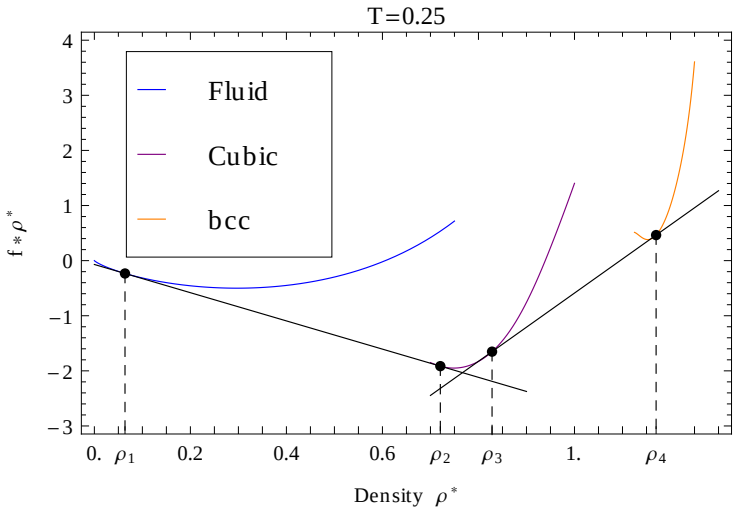

Figure 14: Plot of the common tangents of the three phases. The points where the common tangents touch the lines indicate four points of coexistence, which are shown by the dashed lines.

4.4 Phase Diagram

With knowledge of the free energy the points of coexistence can be found using the common tangent method. The resulting points of coexistence along with the corresponding pressures and chemical potentials are shown in Table 1. In figure 14 the free energy per particle multiplied by the density ($f \cdot \rho^*$) is shown as a function of ρ^*. Points connected by a common tangent in two phases are the densities of the two phasese at the point of coexistence.

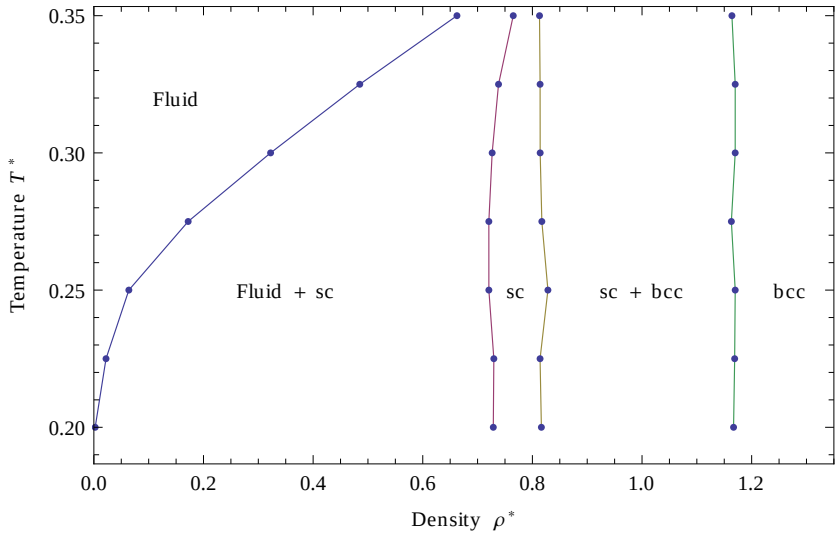

Figure 15: Phase diagram of the octahedral patchy particle system.

Using the common tangent method the densities in which a phase is stable can be found. Repeating this procedure for temperatures within the range we are interested in, the phase diagram can be obtained. The phase diagram in the temperature and density representation is plotted in figure 15. One point of interest is that the stable region of the simple cubic crystal phase seems to shrink at higher temperatures. Recalling that for the simulations at $T^* = 0.4$ the simple cubic crystal phase has been found to either melt or transition into another phase, it is to be expected that the region of stability for the simple cubic crystal phase will diminish somewhere between $T^* = 0.35$ and $T^* = 0.4$. Above this temperature it is likely that a phase coexistence will occur between the fluid and bcc phase. Another possibility however is that the stable region of the bcc phase will also disappear. Since an increase in

T^*	ρ_1	ρ_2	ρ_3	ρ_4	μ_1	p_1	μ_2	p_2
0.2	0.0024	0.7287	0.8164	1.167	-6.014	-0.0024	3.0463	-6.9757
0.225	0.0222	0.7297	0.814	1.169	-4.1055	-0.0147	4.775	-6.8418
0.25	0.0638	0.7206	0.8283	1.17	-2.5601	-0.0698	6.191	-6.7798
0.275	0.172	0.7206	0.8172	1.163	-1.1259	-0.231	7.4741	-6.8459
0.3	0.3224	0.7266	0.8142	1.17	0.4106	-0.6121	8.5701	-6.9135
0.325	0.4851	0.7382	0.814	1.17	2.404	-1.4244	9.324	-6.8031
0.35	0.6624	0.7651	0.813	1.164	5.4871	-3.1965	10.1027	-6.8428

Table 1: Data for the coexistence points obtained through the common tangent method for several temperatures T^*. The coexistence points for the fluid-sc phases are given by ρ_1 and ρ_2 respectively, along with chemical potential μ_1 and pressure p_1. The coexistence points for the sc-bcc phases are given by ρ_3 and ρ_4 respectively, along with chemical potential μ_2 and pressure p_2.

temperature results in a decrease in the interaction strength between patches, at high temperatures the system will approach the hard sphere system. It is therefore quite possible that the face-centered cubic phase will have a stable density region at these temperatures.

5 Conclusions

Through NPT simulations the equations of state have been determined for the fluid, simple cubic crystal and bcc crystal phases for the octahedrally arranged patchy particles. It has been found that at temperatures below $T^* = 0.2$, the fluid phase is only stable at a very low density due to the fact that patch-antipatch interactions are very strong in this temperature range. On the other hand, at a temperature of $T^* = 0.4$, both the crystals have been found to experience melting. In fact, at this temperature the simple cubic crystal phase has not been found to be stable at any pressure measured. The fact that the bcc crystal phase has also been observed to melt occasionally suggests that the region of stability for this crystal phase will also decrease. Since an increase in temperature decreases the patch interaction strength, the system approaches the hard sphere ensemble at higher temperatures. It is therefore expected that above the melting temperature of the crystals the

stable density region of the fcc crystal phase will increase and eventually dominate the stable density regions of the crystal phases.

References

[1] J. Chang, A.M. Lenhoff, and S.I. Sandler. Determination of fluid–solid transitions in model protein solutions using the histogram reweighting method and expanded ensemble simulations. *The Journal of chemical physics*, 120:3003, 2004.

[2] Enrique de Miguel. Estimating errors in free energy calculations from thermodynamic integration using fitted data. *Journal of Chemical Physics*, 129(214112), 2008.

[3] Nicolas Dorsaz, Laura Filion, Frank Smallenburg, and Daan Frenkel. Spiers memorial lecture: Effect of interaction specificity on the phase behaviour of patchy particles. *Faraday Discussions*, 2012.

[4] Daan Frenkel and Berend Smit. *Understanding Molecular Simulation. From Algorithms to Applications*. Academic Press, 2nd edition, 2006.

[5] N. Kern and D. Frenkel. Fluid–fluid coexistence in colloidal systems with short-ranged strongly directional attraction. *The Journal of chemical physics*, 118:9882, 2003.

[6] M. Maldovan and E.L. Thomas. Diamond-structured photonic crystals. *Nature materials*, 3(9):593–600, 2004.

[7] Eva G. Noya, Carlos Vega, and Enrique de Miguel. Determination of the melting point of hard spheres from direct coexistence simulation methods. *Journal of Chemical Physics*, 128(154507), 2008.

[8] A.B. Pawar and I. Kretzschmar. Multifunctional patchy particles by glancing angle deposition. *Langmuir*, 25(16):9057–9063, 2009.

[9] JM Polson, E. Trizac, S. Pronk, and D. Frenkel. Finite-size corrections to the free energies of crystalline solids. *The Journal of Chemical Physics*, 112:5339, 2000.

[10] W.H. Press, S.A. Teukolsky, W.T. Vetterling, and B.P. Flannery. Numerical recipes in c: the art of scientific computing. 2. *Cambridge: CUP*, 1992.

[11] F. Romano, E. Sanz, and F. Sciortino. Phase diagram of a tetrahedral patchy particle model for different interaction ranges. *Journal of Chemical Physics*, 132(184501), 2010.

[12] W.R. Smith and I. Nezbeda. A simple model for associated fluids. *The Journal of chemical physics*, 81:3694, 1984.

[13] C. Vega, E. Sanz, J. L. F. Abascal, and E. G. Noya. Determination of phase diagrams via computer simulation: methodology and applications to water, electrolytes and proteins. *Journal of Physics: Condensed Matter*, 20(153101), 2008.